# Regional evaluation of an advanced very high resolution radiometer (AVHRR) two-channel aerosol retrieval algorithm

Tom X.-P. Zhao,[1,2] Oleg Dubovik,[3] Alexander Smirnov,[3] Brent N. Holben,[4] John Sapper,[5] Christophe Pietras,[6] Kenneth J. Voss,[7] and Robert Frouin[8]

[1]  Advanced Very High Resolution Radiometer (AVHRR) aerosol optical thickness retrieval over the ocean is one of the two existing sources of long-term global satellite aerosol measurements (Total Ozone Mapping Spectrometer aerosol data set is the other). To make this 20-year historical data more useful for climate studies, the quality of the data (or the performance of the retrieval algorithm) has to be systematically evaluated. In this paper, as a continuation of our previous global validation effort, we present regional validation results for an AVHRR independent two-channel aerosol retrieval algorithm by comparing the retrievals with observations from the Aerosol Robotic Network (AERONET). The bias and the random errors of the retrieval algorithm applied to NOAA-14/AVHRR observations were determined and documented for key aerosol types (including biomass-burning, urban/industrial, desert dust, and marine). As a by-product of the validation, effective refractive indexes of the key aerosol types were also statistically determined through sensitivity analysis. The global and regional validations indicate that the new independent two-channel algorithm (with a globally unified aerosol model) performs well in the sense of the global mean. However, improvements are necessary to make the retrieval sensitive to aerosol types and to capture aerosol regional variations. The results will facilitate the utilization of long-term AVHRR aerosol products in climate studies and will provide guidance for improving aerosol retrievals from future NOAA satellite instruments.    *INDEX TERMS:* 0305 Atmospheric Composition and Structure: Aerosols and particles (0345, 4801); 0345 Atmospheric Composition and Structure: Pollution—urban and regional (0305); 0365 Atmospheric Composition and Structure: Troposphere—composition and chemistry; 0360 Atmospheric Composition and Structure: Transmission and scattering of radiation; 4801 Oceanography: Biological and Chemical: Aerosols (0305); *KEYWORDS:* aerosol, retrieval, validation

[1]Cooperative Institute for Research in the Atmosphere, Colorado State University, Fort Collins, Colorado, USA.
[2]Also at E/RA1, RM 7121, WWBG, NOAA/NESDIS/ORA, Camp Springs, Maryland, USA.
[3]Goddard Earth Sciences and Technology Center, University of Maryland Baltimore Campus, Goddard Space Flight Center, Greenbelt, Maryland, USA.
[4]Laboratory for Terrestrial Physics, NASA/GSFC, Greenbelt, Maryland, USA.
[5]NOAA/NESDIS/OSDPD, Suitland, Maryland, USA.
[6]SAIC, NASA/GSFC, Greenbelt, Maryland, USA.
[7]Department of Physics, University of Miami, Coral Gables, Florida, USA.
[8]Scripps Institution of Oceanography, University of California San Diego, La Jolla, California, USA.

## 1. Introduction

[2]  It has been widely recognized that aerosols cause large uncertainties in assessing the radiative forcing of climate by atmospheric constituents [*Intergovernmental Panel on Climate Change*, 2001]. To fully understand the climate effects of aerosols, the mean aerosol properties have to be determined over a long-term period and on a global scale. Satellites are a unique source of long-term observations of global aerosols [*King et al.*, 1999; *Kaufman et al.*, 2002], but only two long-term satellite aerosol products are available now. The first is derived from about 20 years of Total Ozone Mapping Spectrometer (TOMS) measurements in the UV and visible channels [*Herman et al.*, 1997; *Torres et al.*, 1998; *Hsu et al.*, 1999; *Torres et al.*, 2002]. The second is based on about 20 years of AVHRR observations in the visible and near IR channels [*Stowe et al.*, 1997; *Husar et al.*, 1997; *Higurashi et al.*, 2000; *Geogdzhayev et al.*, 2002; *Mishchenko et al.*, 2003]. They supply global

distributions of various aerosol parameters (including aerosol absorption index and aerosol optical thickness from TOMS and aerosol optical thickness and aerosol Ångström wavelength exponent from AVHRR) determined by the nature of their retrieval algorithms, which depends further on the design of the TOMS and the AVHRR instruments. Although the AVHRR-derived aerosol parameters and their accuracy are limited compared to those obtained from more recent and advanced instruments (such as MODIS and MISR), a retrospective 20-year data is still a precious resource for aerosol climate studies.

[3] However, one important issue that has to be considered before the long-term historical aerosol data can be effectively applied in the study of climate change is its accuracy. In other words, the aerosol products should be validated carefully (at both global and regional scales) and the error budgets should be well documented. The global Aerosol Robotic Network (AERONET [*Holben et al.*, 1998]) provides a unique opportunity for global and regional validation of satellite aerosol retrievals of various satellite sensors. Data from this network provide globally distributed and quality assured observations of aerosol spectral optical thickness, aerosol size distribution, etc., in a manner suitable for integration with satellite data [see, e.g., *Dubovik and King*, 2000; *Holben et al.*, 2001; *Smirnov et al.*, 2002b, 2003; *Dubovik et al.*, 2002a]. Thus AERONET measurements provide an ideal ground "truth" data set for long-term validation of satellite aerosol retrievals. In this paper, we will focus on the validation of an AVHRR independent two-channel aerosol retrieval algorithm. This simple algorithm also allows us to do sensitivity studies, based on the validation, to statistically estimate the optical properties (such as refractive index) of key aerosol types (including biomass-burning aerosol, urban/industrial aerosol, desert dust aerosol, and marine aerosol) in the retrospective analysis of AVHRR observations. Thus, the common limitation of using a globally unified aerosol model in the retrieval scheme, due to only a few retrieval channels, can be somewhat overcome.

## 2. Two-Channel Aerosol Retrieval Algorithm

[4] The operational NOAA/NESDIS AVHRR aerosol retrieval algorithm provides estimates over the ocean of aerosol optical thickness ($\tau$) in the visible (0.63-$\mu$m) and near infrared (0.83-$\mu$m) channels of AVHRR, assuming the molecular atmosphere, aerosol microphysics, and surface reflectance are known [*Stowe et al.*, 1997; *Ignatov and Stowe*, 2000]. In practice, the relationship between aerosol optical thickness, $\tau$ and dimensionless reflectance, $\rho$ (radiance normalized to solar flux at the top of the atmosphere) is described by a four-dimensional lookup table (LUT), precalculated for different $\tau$, solar and viewing geometries using a radiative transfer model. The clear-sky radiance of AVHRR in channel 1 ($\lambda_1 = 0.63$-$\mu$m) and 2 ($\lambda_2 = 0.83$-$\mu$m) is input to the retrieval scheme. Aerosol optical thickness ($\tau_1$ and $\tau_2$) are retrieved independently from both channels and the aerosol Ångström wavelength exponent $\alpha$, an indication of aerosol particle size, can be deduced using the relationship $\alpha = -\ln(\tau_1/\tau_2)/\ln(\lambda_1/\lambda_2)$. For this reason the algorithm is described as an "independent" two-channel algorithm. The retrieval is performed for (1) solar zenith angle $\theta_s < 70°$ and view zenith angle $\theta_v < 60°$ to minimize atmospheric curvature effects; (2) glint angle $\eta > 40°$ to avoid sun glint contamination; (3) relative azimuth angle $\varphi_{sv} > 90°$ (the antisolar side of satellite orbit) to include only back scattering.

[5] The AVHRR two-channel aerosol retrieval algorithm used in this study is evolved from the second generation of NOAA/NESDIS operational aerosol retrieval algorithm [*Stowe et al.*, 1997; *Ignatov and Stowe*, 2000]. Compared to the second-generation algorithm, some important modifications and improvements have been made:

[6] 1. A more comprehensive and flexible 6S radiative transfer code [*Vermote et al.*, 1997] replaces *Dave*'s [1973] code for the generation of the look up tables (LUTs). In the 6S code, the ocean surface reflectance is treated more realistically as a wavy Fresnel surface with wind driven slopes (including whitecap effects), whereas the Dave code assumed a Lambertian surface with a diffuse glint correction to the aerosol phase function. Wind speed $U$ is set to 7 m/s in our 6S calculation to represent approximately the mean ocean surface roughness.

[7] 2. Unlike using the mono-modal lognormal aerosol size distribution in the second-generation algorithm, a more widely used bimodal lognormal aerosol size distribution is used to account for accumulation and coarse modes. It is expressed as

$$dV(r)/d\ln r = \sum_{i=1}^{2} c_i \exp\left\{-\frac{1}{2}\left[\frac{\ln(r/r_{mi})}{\ln \sigma_i}\right]^2\right\}, \qquad (1)$$

where $V$ and $r$ are the aerosol volume density and particle radius, respectively. The $c_i$ ($i = 1, 2$) are the columnar volume ($\mu m^3/\mu m^2$) of particles per unit cross section of atmospheric column for the fine and coarse modes. The mode radius ($r_{mi}, i = 1, 2$) and standard deviation $\sigma_i$ are $r_{m1} = 0.17$-$\mu$m and $\sigma_1 = 1.96$ for the accumulation mode; $r_{m2} = 3.44$-$\mu$m and $\sigma_2 = 2.37$ for the coarse mode. This model is the same as that adopted by *Higurashi et al.* [2000] for the retrieval of aerosol optical thickness, $\tau$, and Ångström wavelength exponent, $\alpha$, over the ocean from AVHRR observations. We fixed the mode radius and the dispersions for the accumulation and coarse modes of the size distribution throughout the algorithm, since it is difficult to take into account the hygroscopic processes to change these parameters in our algorithm. However, we still allow the small particle fraction ($\gamma_1 = c_1/c$, $c = c_1 + c_2$) or the large particle fraction ($\gamma_2 = c_2/c$) to vary in the sensitivity studies. This is because $\gamma_1$ (or $\gamma_2$) is a more inherent parameter for radiation transfer processes since it is uniquely transformed to Ångström wavelength exponent $\alpha$ [*Mishchenko et al.*, 1999; *Higurashi and Nakajima*, 1999]. Sensitivity studies have been performed based on the validation results (see detailed discussion later) to choose the ideal values for $\gamma_1$ and $\gamma_2$.

[8] However, there are still some aspects of the 6S code that are not sufficient for some aerosol retrieval applications. First, a plane parallel atmosphere is assumed, ignoring earth curvature effects. This may cause errors in aerosol retrieval from limb observations, but is minimized in our retrievals by setting limits on the retrieval geometry ($\theta_s < 70°$ and $\theta_v < 60°$).

**Table 1.** Selected Nine AERONET Stations for the Validation of AVHRR Aerosol Retrieval[a]

| No. | AERONET Station | Latitude, Longitude | Major Aerosol Type[b] | No. of Matchups |
|---|---|---|---|---|
| 1 | Ascension Island | −7.97°, −14.40° | B, M | 80 |
| 2 | Bahrain | 26.32°, 50.50° | D, U/I | 74 |
| 3 | Barbados | 13.17°, −59.50° | D, M, U/I | 47 |
| 4 | Bermuda | 32.37°, −64.68° | U/I, M | 74 |
| 5 | Cape Verde | 16.72°, −22.93° | D | 86 |
| 6 | Dry Tortugas | 24.60°, −82.78° | U/I, M, D | 87 |
| 7 | Kaashidhoo | 4.95°, 73.45° | M, D | 86 |
| 8 | Lanai | 20.82°, 156.98° | M | 8 |
| 9 | San Nicolas | 33.25°, −119.49° | M, U/I | 57 |

[a]Geographical location (latitude, longitude), major aerosol types observed over them, and numbers of matchups found are indicated.

[b]Abbreviations are as follows: B, biomass-burning aerosol; D, dust aerosol; M, marine aerosol; U/I, urban/industrial aerosol.

[9] Second, gaseous absorption and aerosol scattering are decoupled into different layers with the gaseous absorption layer above the aerosol layer in the 6S code [see *Vermote et al.*, 1997]. This approximation works well in AVHRR channel 1 (0.63-μm) since ozone is the major absorber in this channel and is concentrated in the lower stratosphere. However, it will become inadequate for AVHRR channel 2 (0.83-μm) since there is a strong water vapor absorption band (centered at 0.94-μm) in this channel and water vapor is mainly concentrated in the lower troposphere. A correction has been made in the 6S code to reduce the error associated with water vapor absorption by assuming that half of the water vapor in the atmosphere absorbs the aerosol path radiance. This correction works well on average. For specific conditions where the water vapor is located primarily below the aerosol scattering layer, the 6S will still overestimate the absorption effect of water vapor on the backward scattered radiance in AVHRR channel 2. As a result, there is an overestimate in the retrieved aerosol optical thickness in this channel. One will see that some of the inconsistencies in the following analyses for AVHRR channel 2 are associated with the contamination of water vapor absorption.

[10] Third, the public accessible version of the 6S code used in this study is a scalar radiative transfer model and does not consider polarization. Neglecting polarization may result in an error in the aerosol optical thickness retrieval. This polarization effect is most important at low aerosol concentrations since multiple scattering by aerosol particles (mostly associated with high aerosol concentrations) will depolarize the back scattering radiance [see *Lacis et al.*, 1998]. On the basis of the computation of *Lacis et al.* [1998] on the polarization effect for an ocean atmosphere, *Ignatov and Stowe* [2002] estimated the possible error in radiance due to the neglecting polarization. The magnitude is within 3%−5% in AVHRR channel 1 and is much smaller in AVHRR channel 2 at low aerosol load. These errors become even smaller as aerosol optical thickness increases.

[11] Because of the many features of the 6S code and the limited impact of its drawbacks on the AVHRR aerosol retrievals, it was used to replace the old Dave code in the generation of the LUTs for our AVHRR aerosol retrieval. The 6S code is still under improvement by its developer (E. Vermote, personal communication, 2003). New code (accounting for polarization, etc.) can be adopted easily and consistently for use in our aerosol retrieval algorithm when it is available.

## 3. Validation Methodology

[12] The independent two-channel aerosol retrieval algorithm was applied to retrieve aerosol optical thickness, $\tau_{st}$, from the radiances measured by the AVHRR instrument onboard the NOAA14 satellite. The AERONET observations from the automatic CIMEL Sun/sky radiometers [*Holben et al.*, 2001] provide the ground truth used here to evaluate the AVHRR aerosol optical thickness. The AERONET aerosol optical thickness is derived from the CIMEL radiometer measurement of spectral attenuation of the direct solar beam. Its accuracy is much higher (with an uncertainty of 0.01 [*Smirnov et al.*, 2000]) than that derived from a satellite because of two reasons. (1) Unlike satellite aerosol optical thickness retrieval, no aerosol model assumptions are made in the derivation of AERONET aerosol optical thickness based on the Beer-Lambert-Bouger Law. (2) The backward scattering radiances measured from satellite and used for derivation of aerosol optical thickness are "contaminated" by varying surface (land, ocean, cloud) properties [*Tanré et al.*, 1996]. For convenience, we subsequently refer to these solar extinction measurements as sun photometer (SP) data. Only the AERONET aerosol optical thickness, $\tau_{sp}$, is used in our validation since it is highly accurate and directly comparable to the AVHRR aerosol retrieval.

[13] In our validation, the spectral $\tau_{sp}$ is interpolated to the wavelengths of the two AVHRR channels. An optimal interpolation/extrapolation scheme is applied. The scheme is constructed based on sensitivity studies; a detailed description of the technique is given by *Zhao et al.* [2002]. We have selected 9 AERONET island stations (see Table 1), which cover the major regimes of global oceanic aerosol characteristics [cf. *Husar et al.*, 1997]. Three years (1998−2000) of quality assured level 2 AERONET aerosol optical thickness observations [e.g., *Smirnov et al.*, 2002b] are used as ground truth in the validation. Since only eight matchups were found over the Lanai site, we will ignore this site in the following regional validation study.

### 3.1. Matchup Procedure

[14] Our approach is to colocate the AVHRR $\tau_{st}$ with the AERONET $\tau_{sp}$ within an optimum time/space window (±1 hour and a circle with 100-km radius) at selected AERONET stations. A circular area with a 25-km radius around each AERONET station is eliminated from the matchup window to reduce the effect of land surface reflectance. The optimum matchup window is selected from a set of time/space windows based on best correlation of the two observations. A detailed description on the approach is given by *Zhao et al.* [2002]. Scatter diagrams of $\tau_{st}$ versus $\tau_{sp}$ are produced and statistics are calculated from the overpass matchup points. Linear regression analyses are performed, predicting the satellite retrieval values of $\tau_{st}$ as a function of $\tau_{sp}$ in the form of $\tau_{st} = A + B\tau_{sp}$. Retrieval algorithm performance can be evaluated from the resulting four statistical parameters of the linear regression: $A$ (intercept), $B$ (slope), $\sigma$ (standard error), and $R$ (correlation coefficient).

[15] A nonzero intercept ($A \neq 0$) tells us that the retrieval algorithm is biased at low $\tau$ values, which may result from the additive errors associated with calibration and ocean surface reflection. A slope that is different from unity ($B \neq 1$) may result from the proportional error mainly associated with incorrect assumptions in the aerosol model of a retrieval algorithm. The standard error ($\sigma$) represents the magnitude of random errors, which are proportional to radiometric noise, ocean surface reflection variability, and subpixel cloud contamination [see *Stowe et al.*, 1997; *Zhao et al.*, 2002]. In this paper, our focus is on the error due to incorrect assumptions in the aerosol model of the retrieval algorithm since the errors associated with calibration, ocean surface reflection, and subpixel cloud contamination have been studied separately by *Zhao et al.* [2002, 2003a].

[16] In order to understand the error due to incorrect aerosol model assumption, the linearized single-scattering approximation of reflectance $\rho$ in each channel is introduced, which gives

$$\tau_{st} = 4\mu_s\mu_v \frac{\rho}{\omega P}, \qquad (2)$$

where $\mu_s$ and $\mu_v$ are the cosines of solar and viewing zenith angles; $P$ and $\omega$ are the aerosol phase function and single scattering albedo. Note that ($\omega P$) participates in the equation as a multiplicative term. This suggests that departure from unity for the slope $B$ in the regression formula $\tau_{st} = A + B\tau_{sp}$ comes mainly from uncertainties in the aerosol model. A detailed description of the approach and the physical rationale behind it are given by *Zhao et al.* [2002].

## 3.2. Aerosol Model Adjustment

[17] There are only two channels (0.63-$\mu$m and 0.83-$\mu$m) are available from AVHRR for aerosol retrievals. As a result, only two aerosol optical properties can be derived independently from AVHRR ($\tau_1$ and $\tau_2$ in our case) with strong assumptions for the aerosol model [cf. *Mishchenko et al.*, 1999], including size distribution and refractive index. Aerosol optical parameters, such as phase function $P$ and single scattering albedo $\omega$, also depend on the aerosol model (size distribution and refractive index). Thus, equation (2) suggests an optimum aerosol model may be determined from validations for a set of size distributions and refractive indexes selected beforehand. In theory, the size distribution and refractive index that gives best slope ($B \sim 1$) in the regression analysis of $\tau$ validation should be the solution. The sensitivity of satellite $\tau$ retrieval on the assumption of aerosol size distribution (SD) and refractive index (RI) is also different. Thus it further becomes possible in the validation to fix the size distribution and determine the refractive index (or vice versa) over the locations where surface ground truth of $\tau$ is available.

[18] The only remaining issue is which model parameters (SD or RI) should be fixed. Since the approach proposed here is based on adjusting the AVHRR aerosol optical thickness to match the AERONET measurement, a reasonable choice would be the parameter that has the least effect on the aerosol optical thickness retrieval. *Mishchenko et al.* [1999] performed comprehensive sensitivity studies of aerosol model parameters (size distribution, refractive index, etc.) on the global monthly mean AVHRR retrievals of aerosol optical

thickness $\tau$ and size parameters (Ångström wavelength exponent $\alpha$ and effective radius $r_{eff}$). They found that two very different aerosol size distributions resulted in monthly mean values of $\tau$ that were remarkably similar globally, mostly within ±10% of each other. However, the monthly mean values of $r_{eff}$ were in much worse agreement, differing by more than a factor of 2. The differences in the monthly mean values of $\alpha$ were significantly less than that of $r_{eff}$.

[19] They also found that by changing the aerosol refractive index, especially the imaginary part, the monthly mean $\tau$ can be very different in some locations but the differences in $\alpha$ were small. For example, reducing the imaginary part of the aerosol refractive index from 0.005 to 0.002, decreased $\tau$ up to 25% in areas dominated by larger aerosols as well as in areas with heavy aerosol loads. They concluded the use of a globally unified aerosol refractive index could result in significant systematic regional and/or seasonal errors in AVHRR $\tau$ retrieval. Their results clearly indict the effect of aerosol size distribution on AVHRR $\tau$ retrieval is much less than that of aerosol refractive index.

[20] Therefore, in our analysis the aerosol size distribution will be fixed and the aerosol refractive index will be adjusted to provide a match of $\tau_{st}$ with $\tau_{sp}$. To further minimize the impact of fixing aerosol size distribution on $\tau$ retrieval, the widely used bimodal lognormal size distribution (equation (1)) is used. The selection of fine and coarse mode fractions ($\gamma$) is also based on the physical rationale of the phase function effect alluded in equation (2) and the $\gamma$ value chosen (see below) is also close to the long-term global mean value of AERONET measurements. This approach is only feasible for a simple and straightforward retrieval algorithm (such as this AVHRR two-channel aerosol retrieval algorithm) since many tedious manipulations and great computation load are avoided. The following two-steps approach is adopted in practice.

[21] In the first step, a global validation is performed without separating aerosol types. That is all matchups obtained over the 9 AERONET stations are lumped together to form a "global" (or first order) validation. The rationale behind this is the expectation that, at a minimum, a satellite aerosol retrieval algorithm should perform reasonably well at least in the "global" sense. The aerosol model determined in the global validation can be considered as a model of the global mean and is used as the baseline aerosol model in the next step of regional validation. The concept of global validation is further described by *Zhao et al.* [2002, 2003a]. Before adjusting the aerosol model, the retrieval algorithm is optimized for systematic errors by adjusting the surface reflectance to give the best intercept ($A \sim 0$) in the validation regression analysis [see *Zhao et al.*, 2002, 2003a]. In general, the surface reflectance is adjusted to satisfy $A < 0.05$ in the global validation since the accuracy of AVHRR $\tau$ retrieval is about this value. However, for regional validation, this value can be relaxed to 0.1 at some island stations due to a relatively strong coastal effect on the surface reflectance. The purpose is to minimize the retrieval errors associated with sources other than aerosol model so that the retrieval error due to the aerosol model is enhanced.

[22] For this global validation the refractive index $n = n_r - in_i$ is initially fixed to the commonly used value of $1.5 - i0.005$ [e.g., *Mishchenko et al.*, 1999; *Higurashi et al.*,
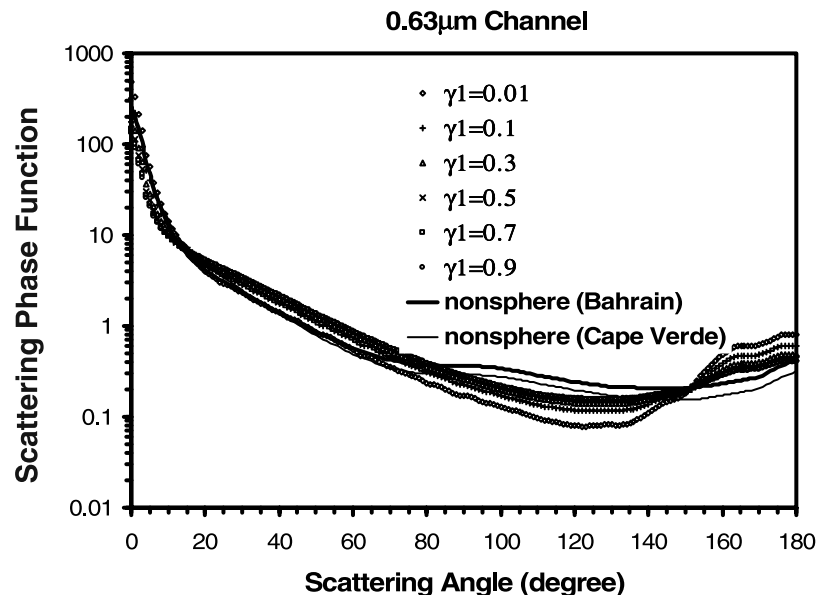
**Figure 1.** Aerosol phase functions calculated from Mie theory in AVHRR 0.63-μm channel for various size distributions defined by the fraction of the small particle component ($\gamma_1$) in a bimodal lognormal size distribution. The typical phase functions of nonspherical particles derived from AERONET measurements (interpolated to the satellite retrieval channel) at Cape Verde and Bahrain are also displayed for comparison. See color version of this figure in the HTML.

2000] for the two AVHRR channels. Then, the size distribution is varied by changing the ratio of accumulation and coarse modes (or change $\gamma_1$ from 0.1 to 0.9 in steps of 0.2). For each $\gamma_1$ value, a new LUT is produced for the two channels, a new $\tau_{st}$ is retrieved, matchups are found, and the validation regression is performed. It is found that the validation results are not sensitive to $\gamma_1$ in the range of $0.3 \leq \gamma_1 \leq 0.9$, which has also been noticed by *Durkee et al.* [1991] and *Gross et al.* [2003]. This is because the aerosol scattering phase function is not sensitive to $\gamma_1$ value in the range of $0.3 \leq \gamma_1 \leq 0.9$ as demonstrated in Figure 1, except when the scattering angle ($\Theta$) is larger than 160°. As mentioned above, retrieved global monthly mean values of $\tau$ found to be insensitive to the aerosol size distribution [*Mishchenko et al.*, 1999]. These observations support a globally unified $\gamma_1$ (or $\gamma_2$) value being used in our AVHRR aerosol optical thickness retrievals. The mean $\gamma_1$ value derived from AERONET observations in maritime environment is about 0.24 (see Table 4 [*Smirnov et al.*, 2002b]). Thus, from the five $\gamma_1$ cases defined beforehand for our sensitivity studies, $\gamma_1 = 0.3$ is selected as our baseline value.

[23] With $\gamma_1$ fixed to the baseline value (0.3), $n_r$ is then varied from 1.34 to 1.60 with a step of 0.01 and $n_i$ from 0.000 to 0.03 with a step of 0.001. The study on sensitivity to aerosol model is focused here on aerosol scattering and absorption properties (or on refractive index) since the sign (cooling or heating) of aerosol radiative forcing is mainly determined by the scattering and absorption properties of aerosol particles. The best solution is sought according to the regression parameter $B$ for the two AVHRR channels among all the combinations of $n_r$ and $n_i$. This is because $B$ is very sensitive to the

value of aerosol refractive index (especially the imaginary part $n_i$) as indicated by the term of $\omega P$ in equation (2) and the discussions above. It was also noticed in our calculation that the change of $B$ with $n_i$ and $n_r$ is in opposite trend ($B$ increases when $n_i$ increases and $n_r$ decreases). In our current analysis, the pair of $n_r$ and $n_i$ that has $B$ closest to unity among all the combinations of preselected $n_r$ and $n_i$ are pinpointed as our optimal solution, which is also used to represent the global mean values of aerosol refractive index. The final $n_r$ and $n_i$ selected in this simplified procedure is somewhat subjective. This is because a priori knowledge of the approximate dynamic range of $n_r$ and $n_i$ values of the key aerosol types is needed to make the final selection when the solution is not unique. A more objective approach will be discussed later.

[24] In the second step, a regional validation is performed. That is matchups at individual AERONET station are validated separately. Global mean values of $n_r$ and $n_i$, determined in the first step, are used as baseline values. Collection of 3 years of data makes this regional validation possible since sufficient matchups (see Table 1) can be found for each selected AERONET station except Lanai. The $\gamma_1$ is fixed to the global baseline value ($\gamma_1 = 0.3$) in the regional validation for most of the AERONET sites selected except for the two dust sites (Cape Verde and Bahrain), where $\gamma_1 = 0.01$ is used instead. At these two sites the aerosol coarse mode dominates [*Tanré et al.*, 2001; *Dubovik et al.*, 2002a]. The sensitivity study performed on the refractive index in the global validation is repeated for each AERONET station to determine the optimal refractive index. Since the prevailing aerosol types over each AERONET station are different [*Smirnov et al.*, 2002a, 2002b; *Dubovik et al.*, 2002a], the $n_r$ and $n_i$ values for the prevailing aerosol
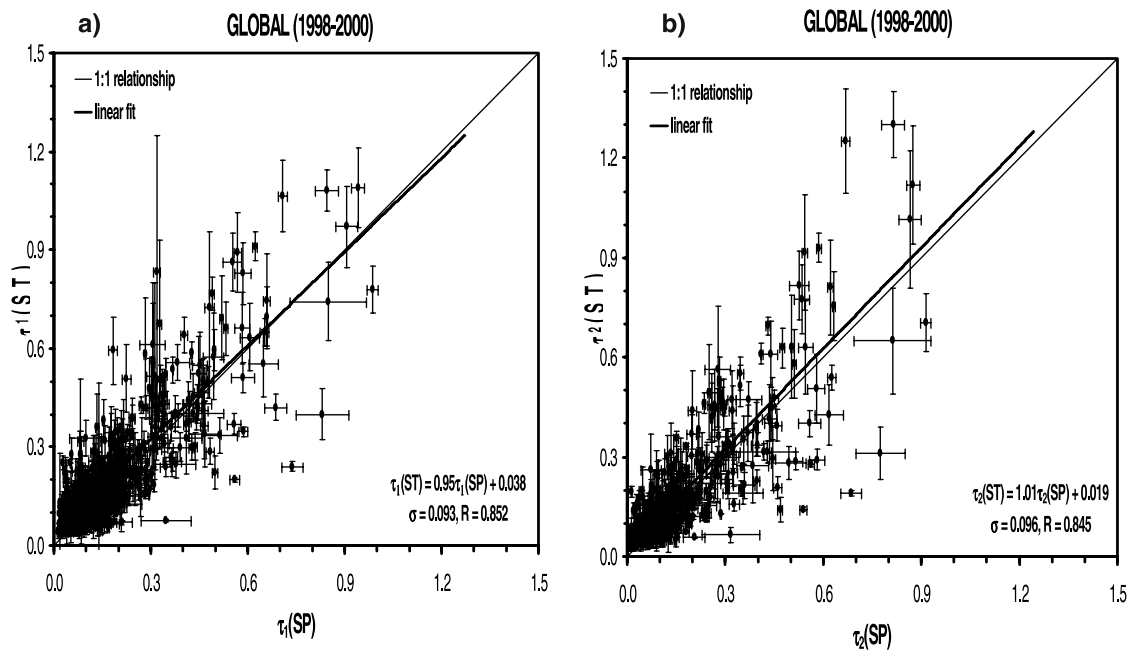
**Figure 2.** Scatterplots of (a) $\tau_1$, (b) $\tau_2$, and the corresponding linear regression lines (bold) and parameters from the global validation of 3-year AVHRR-AERONET matchup data. The general straight line represents 1:1 relationship. Horizontal and vertical error bars are ±1 standard deviation, which are computed for each individual matchup point from all the matchup AVHRR (or AERONET) records found in one overpass. In general, we do not anticipate a large standard deviation (which implies large variation of the AVHRR or AERONET $\tau$ values in the matchup window).

types (including biomass-burning, urban/industrial, desert dust, and marine aerosol) can be determined and compared with the AERONET values.

## 4. Results and Discussions

### 4.1. Global Validation

[25] The optimal global validation result from the sensitivity study is given in Figure 2, which shows the scatterplot of all $\tau_1$ and $\tau_2$ matchups between AVHRR and CIMEL radiometers during 1998–2000. Linear regression equations are also provided in the figure. The regression statistics are summarized in the first row of Table 2. The standard error of the regression provides an estimate of the random error. The resulting linear regression slopes and intercepts are used to estimate the systematic biases at the mean and two extreme $\tau$ values and the results are summarized in the first row of Table 3. Compared to the AERONET observations for global mean conditions, the AVHRR-retrieved $\tau$ values are biased high by 0.03 at both 0.63-μm and 0.83-μm channels, with random errors of ±0.11 and ±0.10, respectively. In terms of systematic biases for the global mean conditions, the two-channel retrieval algorithm works very well considering a single aerosol model is assumed in the retrieval algorithm. The random errors, however, are a bit large, mainly due to the regional variations of aerosol types as indicated in our previous validation work [*Zhao et al.*, 2002]. This will be further examined in the following regional validation.

[26] The corresponding optimal refractive index of the aerosol model determined from the global sensitivity

studies is given in the first row of Table 4. The real part ($n_r = 1.45$) is relatively small while the imaginary part ($n_i = 0.005$ at 0.63-μm and $n_i = 0.007$ at 0.83-μm) agrees well with those widely used values ($n_r = 1.50$; $n_i = 0.005$) in the AVHRR satellite aerosol retrievals [e.g., *Higurashi and Nakajima*, 1999; *Geogdzhayev et al.*, 2002]. There is a minor wavelength dependence of $n_i$ for the two AVHRR channels, which has also been observed by *Higurashi et al.* [2000] in the validation of their two-channel AVHRR aerosol retrieval algorithm. This spectral dependence of the imaginary part of the refractive index will be further discussed later.

[27] To further support our approach and to test the derived aerosol model, the aerosol optical thickness at wavelengths shorter (0.44-μm) and longer (1.02-μm) than the two AVHRR retrieval channels (0.63-μm and 0.83-μm) were predicted using the relationship $\tau_\lambda = \tau_{\lambda_0}(\lambda/\lambda_0)^{-\alpha}$ for two cases. The first case is our initial aerosol model ($\gamma_1 = 0.3$; $n_r = 1.50$; $n_i = 0.005$ at 0.63-μm and 0.83-μm) and the second is the final aerosol model solution ($\gamma_1 = 0.3$; $n_r = 1.45$; $n_i = 0.005$ at 0.63-μm and $n_i = 0.007$ at 0.83-μm) from the global validation. Satellite matchup values of $\tau_{\lambda_0 = 0.63 \, \mu m}$ and averaged $\alpha$ (from all matchups) for the two cases were used in the computation. The predicted results of the two cases are compared in Figure 3 as the scatterplots against the AERONET measurements. The linear regression lines and the corresponding formulas are also provided in the figure. It is seen the predicted aerosol optical thickness at 0.44-μm and 1.02-μm using the optimized aerosol model compares much better to the AERONET measurements than those using the initial aerosol model.

**Table 2.** Regression Statistics for the Optimal Global and Regional Validations of AVHRR Aerosol Optical Thickness Retrieval at Selected AERONET Stations

| Satellite Channel, μm | A Value | ΔA Value | B Value | ΔB Value | σ Value | R Value |
|---|---|---|---|---|---|---|
| *Global Ensemble* | | | | | | |
| 0.63 | 0.0313 | 0.0068 | 0.9926 | 0.0289 | 0.1130 | 0.8144 |
| 0.83 | 0.0318 | 0.0059 | 1.0036 | 0.0280 | 0.1029 | 0.8256 |
| *Ascension Island* | | | | | | |
| 0.63 | 0.0533 | 0.0181 | 0.9750 | 0.1257 | 0.0790 | 0.6598 |
| 0.83 | 0.0684 | 0.0165 | 0.9492 | 0.1357 | 0.0706 | 0.6208 |
| *Bahrain* | | | | | | |
| 0.63 | 0.0355 | 0.0314 | 0.9576 | 0.1128 | 0.1299 | 0.7072 |
| 0.83 | 0.0315 | 0.0271 | 1.0063 | 0.1137 | 0.1233 | 0.7219 |
| *Barbados* | | | | | | |
| 0.63 | 0.0252 | 0.0119 | 1.0223 | 0.0811 | 0.0507 | 0.8829 |
| 0.83 | 0.0287 | 0.0118 | 0.9822 | 0.0867 | 0.0526 | 0.8607 |
| *Bermuda* | | | | | | |
| 0.63 | 0.0521 | 0.0209 | 0.9300 | 0.1393 | 0.0492 | 0.6942 |
| 0.83 | 0.0389 | 0.0207 | 0.9346 | 0.1867 | 0.0451 | 0.6647 |
| *Cape Verde* | | | | | | |
| 0.63 | −0.0010 | 0.0310 | 1.0424 | 0.0647 | 0.1506 | 0.8603 |
| 0.83 | −0.0432 | 0.0309 | 0.9774 | 0.0708 | 0.1513 | 0.8330 |
| *Dry Tortugas* | | | | | | |
| 0.63 | 0.0758 | 0.0143 | 0.9590 | 0.0892 | 0.0682 | 0.7789 |
| 0.83 | 0.0537 | 0.0127 | 1.0418 | 0.1198 | 0.0579 | 0.7469 |
| *Kaashidhoo* | | | | | | |
| 0.63 | 0.0620 | 0.0184 | 0.9355 | 0.0958 | 0.0867 | 0.7290 |
| 0.83 | 0.0269 | 0.0121 | 0.9797 | 0.0869 | 0.0524 | 0.7758 |
| *San Nicolas* | | | | | | |
| 0.63 | 0.0885 | 0.0186 | 0.9173 | 0.3562 | 0.0554 | 0.3549 |
| 0.83 | 0.0595 | 0.0089 | 0.9019 | 0.2308 | 0.0325 | 0.4993 |

[28] The above error budgets of the global retrieval are obtained from the validation of aerosol optical thickness derived from the measurement of NOAA-14/AVHRR instrument. They cannot be automatically applied to the historical AVHRR observations from other NOAA polar satellite platforms. This is because radiometric noise and calibration errors of the AVHRR instruments vary for different satellite platforms. However, the derived global mean aerosol model should be less dependent on satellite platforms than the retrieval accuracy since the globally averaged aerosol model is determined after systematic errors (such as calibration errors) included in the intercept (*A*) of the validation regression have been minimized.

## 4.2. Regional Validation

[29] Similar to the global validation, the results of the regional validation have been summarized for each AERONET site in Tables 2, 3, and 4. Aerosols over the sites do not originate only from the ocean. Actually, various aerosols generated over land may prevail over some sites for a quite long period during the year due to atmospheric transport. Therefore it is reasonable to classify the AERONET sites according to the major prevailing aerosol types over them and to examine the validation results accordingly. We divided the nine sites into four groups as indicated in Table 1 (column 4) according to four key

aerosol types: desert dust, biomass burning, urban/industrial, and marine. The results for each group are examined below in detail.

### 4.2.1. Dust Aerosols

[30] Cape Verde, Bahrain, and Barbados are considered as dust aerosol sites in our validation. AERONET measurements have revealed that Cape Verde is impacted strongly by desert dust from the western part of Africa and the Saudi Arabian Peninsula and displays aerosol optical properties more representative of so-called pure desert dust [*Kaufman et al.*, 2001; *Tanré et al.*, 2001; *Dubovik et al.*, 2002a]. Bahrain is dominated by desert aerosols almost year around. However, small particles produced by industrial activity near the Persian Gulf are sometimes present [*Smirnov et al.*, 2002a]. Mineral dust is the major aerosol component during much of the year (maximum in the summer and minimum in the winter) at Barbados because of long-range atmospheric transport [*Prospero*, 1995a, 1995b]. However, other species (such as urban pollutants from Europe) can be present as well, especially during winter [*Li et al.*, 1996]. Thus, among the three dust aerosol sites in our validation, Cape Verde displays the purest dust particles, Bahrain comes second, and Barbados last.

[31] For a typical optical thickness of dust aerosols at Bahrain ($\tau = 0.4$), the systematic errors obtained are 0.02 and 0.03, with random errors of ±0.13 and ±0.12, in the 0.63-μm and 0.83-μm channels, respectively. At Cape Verde, the systematic errors are 0.02 and −0.05 and the random errors are 0.15 in both channels. For typical optical thickness of dust aerosols at Barbados ($\tau = 0.25$), the systematic errors are 0.03 and 0.02, and the random errors are ±0.05 for both channels. We derived a refractive index for dust particles by averaging the refractive indices at the three dust sites. The real part is 1.48 for both 0.63-μm and 0.83-μm channels and the imaginary part is 0.003 and 0.005, respectively. The value of the real part given by *Tanré et al.* [2001] for dust aerosol is 1.46−1.53 and the AERONET value is in the range of 1.48−1.56 [*Dubovik et al.*, 2002a]. Our value agrees well with them, especially with the value given by *Tanré et al.* [2001]. The retrieved imaginary part of the refractive index from *Tanré et al.* [2001] is 0.001−0.003 and the AERONET value is in the range 0.0006−0.003 while the value adopted for several radiative transfer models [*Shettle and Fenn*, 1979; *World Meteorological Organization*, 1983] is 0.008 in the visible based on in situ measurements. Our values are closer to those from AERONET and *Tanré et al.* [2001].

[32] Similar to the global result, the spectral dependence of the imaginary part of the refractive index is also obtained for dust particles. The spectral dependence of the imaginary part has also been obtained from both AERONET data [*Dubovik et al.*, 2002a] and in situ measurements [*Patterson et al.*, 1977; *Sokolik et al.*, 1993; *Koepke et al.*, 1997; *Sokolik and Toon*, 1999], but with an opposite trend (value decreases from short to long wavelengths). The increasing trend with wavelength in our results is probably due to the contamination of water vapor absorption near 0.94-μm in the 0.83-μm spectral band (0.7-μm−1.05-μm) of the AVHRR instrument [*Stowe et al.*, 1997]. Water vapor is generally concentrated below the dust layer for African dusts [*Tanré et al.*, 1992]. The treatment of the water vapor absorption in the 6S code, as mentioned above, will

**Table 3.** Systematic and Random Errors Determined From the Optimal Global and Regional Validations[a]

| Satellite Channel, μm | Systematic Errors | | | |
| | Minimum ($\tau = 0.00$) | Mean ($\tau = 0.15$ at $\lambda_1$) ($\tau = 0.11$ at $\lambda_2$) | Maximum ($\tau = 1.00$) | Random Error (±) |
|---|---|---|---|---|
| *Global Ensemble* | | | | |
| $\lambda_1 = 0.63$ | 0.031 | 0.030 | 0.024 | 0.113 |
| $\lambda_2 = 0.83$ | 0.032 | 0.032 | 0.035 | 0.103 |
| | | | | |
| *Ascension Island* | | | | |
| $\lambda_1 = 0.63$ | 0.053 | 0.050 | 0.028 | 0.079 |
| $\lambda_2 = 0.83$ | 0.068 | 0.063 | 0.018 | 0.071 |
| | | | | |
| *Bahrain* | | | | |
| $\lambda_1 = 0.63$ | 0.036 | 0.029 | −0.007 | 0.130 |
| $\lambda_2 = 0.83$ | 0.032 | 0.032 | 0.038 | 0.123 |
| | | | | |
| *Barbados* | | | | |
| $\lambda_1 = 0.63$ | 0.025 | 0.029 | 0.048 | 0.051 |
| $\lambda_2 = 0.83$ | 0.029 | 0.027 | 0.011 | 0.053 |
| | | | | |
| *Bermuda* | | | | |
| $\lambda_1 = 0.63$ | 0.052 | 0.042 | −0.018 | 0.049 |
| $\lambda_2 = 0.83$ | 0.039 | 0.032 | −0.027 | 0.045 |
| | | | | |
| *Cape Verde* | | | | |
| $\lambda_1 = 0.63$ | −0.001 | 0.005 | 0.041 | 0.151 |
| $\lambda_2 = 0.83$ | −0.043 | −0.046 | −0.066 | 0.151 |
| | | | | |
| *Dry Tortugas* | | | | |
| $\lambda_1 = 0.63$ | 0.076 | 0.070 | 0.035 | 0.068 |
| $\lambda_2 = 0.83$ | 0.054 | 0.058 | 0.096 | 0.058 |
| | | | | |
| *Kaashidhoo* | | | | |
| $\lambda_1 = 0.63$ | 0.062 | 0.052 | −0.003 | 0.087 |
| $\lambda_2 = 0.83$ | 0.027 | 0.025 | 0.007 | 0.052 |
| | | | | |
| *San Nicolas* | | | | |
| $\lambda_1 = 0.63$ | 0.088 | 0.076 | 0.006 | 0.055 |
| $\lambda_2 = 0.83$ | 0.059 | 0.049 | −0.039 | 0.033 |

[a]Systematic biases are estimated using the linear regression slopes and intercepts at mean $\tau$ values and two extremes (minimum $\tau = 0.00$ and maximum $\tau = 1.00$).

overestimate the water vapor absorption in the look-up table for the 0.83-μm spectral band and, as a result, overestimate retrieved aerosol optical thickness for a given radiance. A higher aerosol optical thickness corresponds to stronger aerosol absorption after the validation statistic parameter (slope *B*) is optimized through adjusting the values of $n_i$. This will be tested in future validation studies of the two-channel algorithm using MODIS narrow band radiances as the input. Thus, the imaginary part of refractive index obtained at AVHRR 0.83-μm channel is too uncertain and is listed for reference but will not be discussed in the following.

[33] Relatively large random errors in the two AVHRR channels at Cape Verde and Bahrain sites (compared to the other sites in Table 3) caught our attention. Several attempts were made to reduce them through the above mentioned sensitivity studies without success. The cause may be the nonspherical effect of dust particles at the two sites since this is the major difference of large dust particles from the other aerosol types. In fact, the importance of the nonspherical effects in an AVHRR retrieval of dust particles over desert areas has already been identified by *Mishchenko et al.* [2003]. Typical phase functions of nonspherical particles derived from AERONET measurements at the two dust sites are displayed in Figure 1. It is seen that the features of the phase functions are very different for spherical and non-

spherical particles in the backward scattering directions, especially when the coarse mode becomes dominant. For scattering angles ($\Theta$) between 90° and 150°, the phase function values of nonspherical particles are larger than that of the corresponding spherical particles. However, for $\Theta > 150°$ the trend is reversed. Since $\tau_{st}$ retrieved from the backscattered solar radiance is proportional to the term of $[\omega P(\Theta)]^{-1}$ according to equation (2), the nonsphericity of dust particles may greatly affect the satellite aerosol retrievals.

[34] To test this idea, the typical aerosol size distributions, refractive indexes, and phase functions (interpolated to the satellite channel) derived from the AERONET measurements for nonspherical dust particles at the two sites are used to replace those of spherical particles for the generation of new look-up tables (LUTs) employed in our AVHRR aerosol retrieval algorithm. The validation against the AERONET aerosol retrievals using the new LUTs (based on nonspherical theory) is compared to that derived using the old LUTs (based on Mie theory). The difference in the validation results indicates the nonspherical effect of dust particles on the satellite aerosol retrieval. One example is given in Figure 4, which displays the scatterplot of validation at Cape Verde for the aerosol optical thickness retrieved from the AVHRR 0.63-μm and 0.83-μm channels with both

**Table 4.** Refractive Index Values Determined From the Sensitivity Study of Global and Regional Regression Validations

| Satellite Channel, μm | Real Part $n_r$ | Imaginary Part $n_i$ |
|---|---|---|
| *Global Ensemble* | | |
| 0.63 | 1.45 | 0.005 |
| 0.83 | 1.45 | 0.007 |
| *Ascension Island* | | |
| 0.63 | 1.45 | 0.016 |
| 0.83 | 1.45 | 0.026 |
| *Bahrain* | | |
| 0.63 | 1.5 | 0.003 |
| 0.83 | 1.5 | 0.01 |
| *Barbados* | | |
| 0.63 | 1.45 | 0.005 |
| 0.83 | 1.45 | 0.007 |
| *Bermuda* | | |
| 0.63 | 1.35 | 0.014 |
| 0.83 | 1.35 | 0.014 |
| *Cape Verde* | | |
| 0.63 | 1.5 | 0.002 |
| 0.83 | 1.5 | 0.005 |
| *Dry Tortugas* | | |
| 0.63 | 1.4 | 0.008 |
| 0.83 | 1.4 | 0.004 |
| *Kaashidhoo* | | |
| 0.63 | 1.4 | 0.008 |
| 0.83 | 1.4 | 0.007 |
| *San Nicolas* | | |
| 0.63 | 1.4 | 0.005 |
| 0.83 | 1.4 | 0.003 |

spherical and nonspherical assumptions. The correlation is improved and the random error is reduced when the nonspherical effect is considered. More detailed discussions on the problem are given by *Zhao et al.* [2003b] and *Dubovik et al.* [2002b]. This regional validation indicates the importance of taking into account the effects of nonsphericity in the retrieval of large dust particles from AVHRR measurements.

### 4.2.2. Biomass-Burning Aerosols

[35] Ascension Island is the only site that is influenced by smoke particles from biomass burning in southern Africa in July–September [*Husar et al.*, 1997] because of the westward transport associated with the high-pressure center over the southern Atlantic Ocean. For the global mean aerosol loading condition ($\tau_1 = 0.15$ and $\tau_2 = 0.11$), the systematic errors over this site are 0.05 and 0.06, with random errors of ±0.08 in 0.63-μm channel and ±0.07 in 0.83-μm channel. The real part of the refractive index is 1.45 for both 0.63-μm and 0.83-μm channels and the imaginary part is 0.016 and 0.026, respectively. This is the site (see Table 4) for which the imaginary part of the aerosol refractive index shows the highest value. This is consistent with the fact that smoke from biomass burning is an absorbing aerosol with black carbon produced by combustion. This feature is still maintained over the site after long-range transport of the biomass-burning aerosol in our AVHRR retrieval. The near source values of $n_r$ and $n_i$ from the AERONET measurements are in the range of 1.47–1.52 and 0.009–0.021,

respectively. The exact values depend strongly on the location of the smoke sources [*Dubovik et al.*, 2002a]. Our $n_i$ (0.016) agrees well with the AERONET values, while $n_r$ is slightly smaller than the AERONET values.

[36] A stronger spectral dependence of $n_i$ is obtained here for the biomass-burning aerosols compared to the above dust particles and the global mean aerosols. This is inconsistent with the almost flat spectral feature (or minor increase at longer wavelength) observed from other remote sensing techniques and in situ measurements for smoke particles [e.g., *Koepke et al.*, 1997; *Dubovik et al.*, 2002a; *Procopio et al.*, 2003]. This spectral trend is probably also due to an error in the treatment of water vapor absorption near 0.94-μm in the AVHRR 0.83-μm spectral band.

### 4.2.3. Urban/Industrial Aerosols

[37] Bermuda and Dry Tortugas are categorized as urban/industrial sites in our validation since they are influenced respectively by the urban pollution from the eastern and southeastern United States through dynamic transport [e.g., *Galloway and Whelpdale*, 1987; *Husar et al.*, 1997; *Remer et al.*, 1999]. This transport peaks in springtime, which is consistent with the prevailing westerly winds in the regions. For the global mean aerosol loading condition, the systematic errors for the two AVHRR retrieval channels are 0.04 and 0.03 at Bermuda, 0.07 and 0.06 at Dry Tortugas. The corresponding random errors are ±0.05 for both channels at Bermuda, ±0.07 and ±0.06 at Dry Tortugas.

[38] The real part of the refractive index at the two sites is 1.35 at Bermuda and 1.40 at Dry Tortugas. These values are comparable with the TARFOX experiment estimates (1.33–1.45) and slightly lower than AERONET measurement (1.39–1.44). The imaginary part of the refractive index estimated from the TARFOX experiment is in the range of 0.001–0.008 [*Redemann et al.*, 2000]. Our values are relatively high with 0.014 for both channels at Bermuda and 0.008 and 0.004 at Dry Tortugas. Large variations in $n_i$ have been observed in the AERONET values for urban/industrial aerosols [*Dubovik et al.*, 2002a]. For example, very weak absorption ($n_i = 0.003$) has been found for the pollution haze at Goddard Space Flight Center, Maryland. However, the pollution of Mexico City ($n_i = 0.014$) and aerosols over the Maldives/INDOEX ($n_i = 0.011$) and Creteil/Paris France ($n_i = 0.009$) display strong absorption comparable to African savanna smoke. The observed wide variability of urban/industrial aerosol absorption is due to differences in fuel types, emission conditions, long-range transport and meteorological conditions. For example, Africa dust particles are transported to the southeastern United States in summer [*Herman et al.*, 1997; *Husar et al.*, 1997]. This may explain somewhat the high $n_r$ and the low $n_i$ values at Dry Tortugas (compared to Bermuda).

### 4.2.4. Marine Aerosols

[39] The marine aerosol in our definition is the particles with maritime origin. The concentration of marine aerosols is usually low. Kaashidhoo, Lanai, and San Nicolas are the three sites that are considered as the marine stations in our validation, even though some influence of long-range transport of dust and pollution may also be present occasionally. As we mentioned above, Lanai is omitted in our discussion due to the limited number of matchup points. For the global mean aerosol concentrations, the systematic errors we obtained for the two AVHRR channels are 0.05 and 0.03
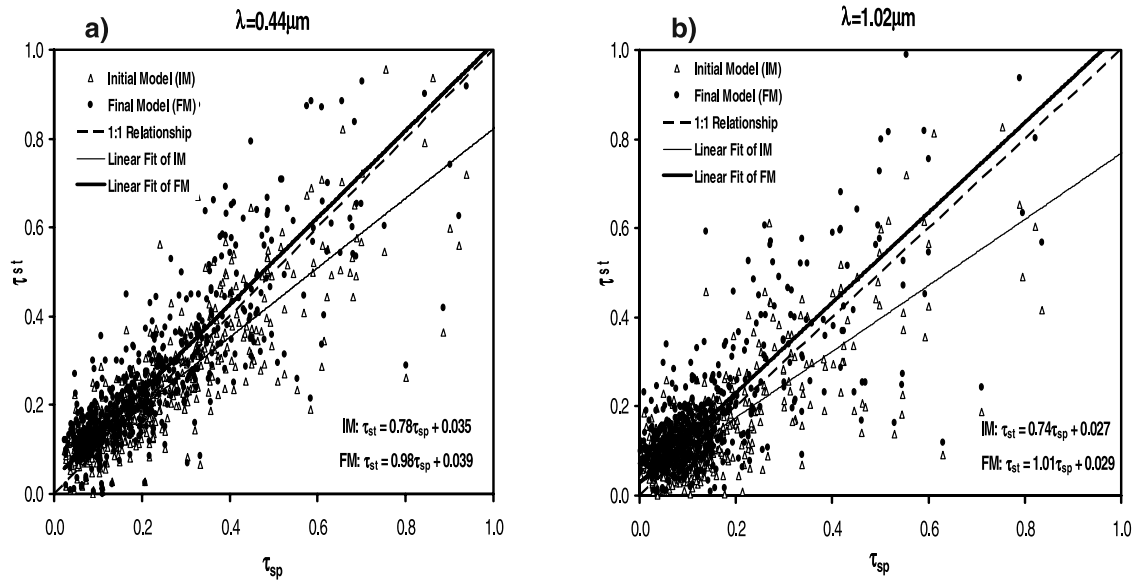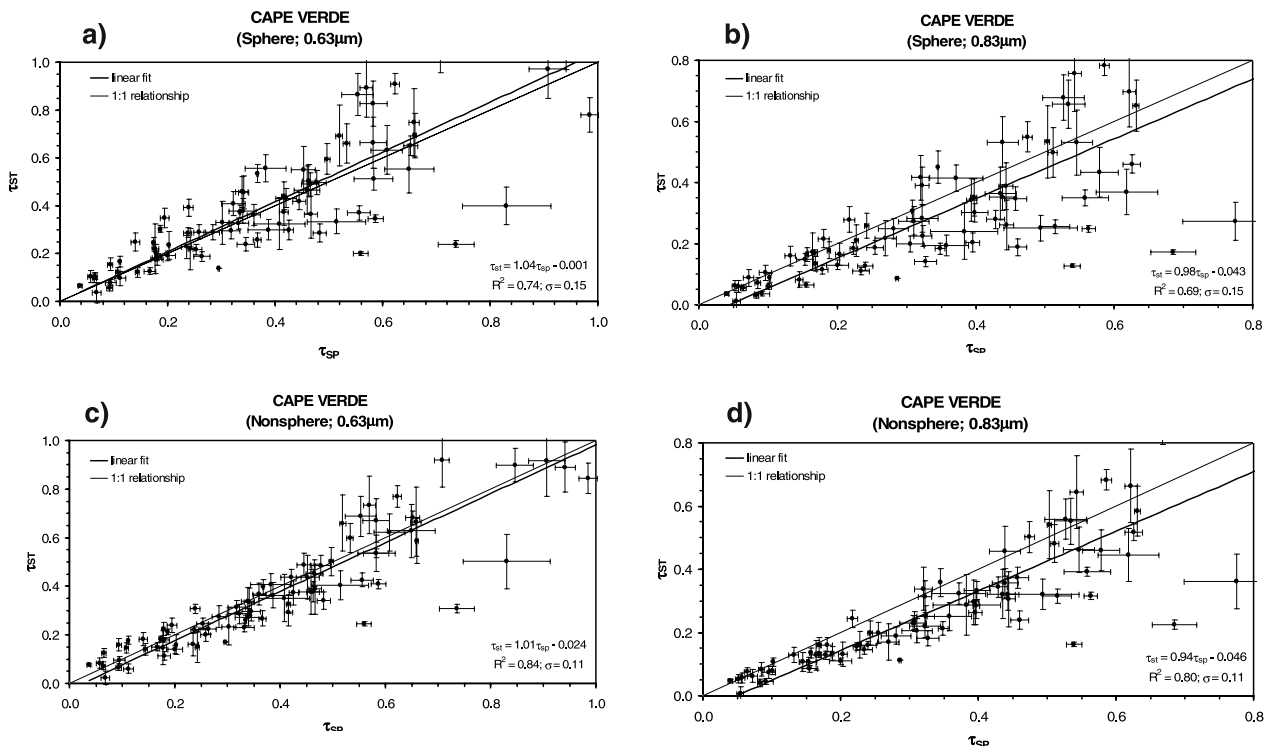
**Figure 3.** Scatterplots of two AVHRR aerosol optical thicknesses versus AERONET values at (a) 0.44-μm and (b) 1.02-μm for the global AVHRR-AERONET matchup points. The two satellite data were predicted respectively by using the relationship $\tau_\lambda = \tau_{\lambda_0}(\lambda/\lambda_0)^{-\alpha}$ for two cases: (1) the Initial aerosol Model (IM: $\gamma_1 = 0.3$; $n_r = 1.50$; $n_i = 0.005$ at 0.63-μm and 0.83-μm) adopted in the global validation; (2) the Final aerosol Model solution (FM: $\gamma_1 = 0.3$; $n_r = 1.45$; $n_i = 0.005$ at 0.63-μm and $n_i = 0.007$ at 0.83-μm) in the global validation. The linear regression lines and the formulas along with the 1:1 relationship are also provided.



**Figure 4.** Scatterplots of matchup data at Cape Verde for the aerosol optical thickness retrieved from the radiance of AVHRR 0.63-μm and 0.83-μm channels with both spherical and nonspherical assumptions. Linear regression lines have also been displayed along with the regression parameters.

at Kaashidhoo, 0.08 and 0.05 at San Nicolas. The corresponding random errors are ±0.09 and ±0.06 at Kaashidhoo, ±0.05 and ±0.03 at San Nicolas.

[40] The real part of the refractive index at the two sites are the same 1.40 while the AERONET value is $1.44 \pm 0.02$ at Kaashidhoo and $1.35 - 1.40$ at San Nicolas. The imaginary part of the refractive index estimated from our validation is 0.008 and 0.007 at Kaashidhoo and 0.005 and 0.003 at San Nicolas. The corresponding AERONET data is $0.011 \pm 0.007$ at Kaashidhoo and $0.004 - 0.006$ at San Nicolas. Our values of the refractive index compare reasonably well with the AERONET data. The difference of the refractive index values between these two sites may be associated with the difference of the contamination due to long-range transport. For example, mineral dust from the Saudi Arabian Peninsula is observed over Kaashidhoo in summer due to the transport of monsoon circulation [*Ackerman and Cox*, 1989]. Air pollution over the western coast of the United States may also disperse to San Nicolas Island in summer due to the offshore wind pattern.

[41] Similar to the global validation, the error budgets of the aerosol retrieval obtained from the regional validation are also dependent on the satellite platform. However, the derived values of aerosol refractive index for the key aerosol types are less dependent on satellite platforms since they are determined after the systematic errors (including sensor calibration error) included in the intercept ($A$) of the validation regression have been minimized. Since the prevailing aerosol types over an AERONET site change due to seasonal variations in the wind patterns, our categorization of the AERONET sites according to their prevailing aerosol types cannot be precise. This may explain most of the difference between our refractive indexes for the key aerosol types and the AERONET values given by *Dubovik et al.* [2002a], which are more representative of the values near the sources of the key aerosol types. The values of the aerosol refractive indexes derived here are more in a sense of statistic mean for 3-year data. Statistics could be slightly different for a longer (or a different) period. Therefore our values of aerosol refractive indexes for the key aerosol types should be considered as effective values. A more detailed categorization according to season is required in our regional validation to produce values in better agreement with the AERONET observations. The number of matchups found in the 3-year analysis is still not sufficient for this purpose. More data will be collected in the future to obtain sufficient matchups for each season, so that the seasonal variations of aerosol refractive index can be determined.

## 5. Summary and Conclusions

[42] We have presented global and regional validation results for an independent two-channel AVHRR aerosol retrieval algorithm (which evolved from the second generation of NOAA/NESDIS operational aerosol retrieval algorithm) by comparing the satellite AVHRR estimates with surface AERONET measurements. The bias and random errors of the retrieval algorithm for the optimized aerosol models have been determined and documented for four key

aerosol types (including biomass-burning, urban/industrial, desert dust, and marine aerosol) observed by the NOAA-14/AVHRR over oceans. These error budget estimates represent the performance of NOAA-14/AVHRR aerosol retrieval only and they may not apply to the 20-year AVHRR historical records.

[43] As a by-product of the validation, refractive indexes of the key aerosol types have also been estimated statistically for the first time in an AVHRR aerosol retrieval. The values in most cases are in good agreement with those derived from AERONET observations. The inconsistent imaginary parts of the refractive indexes in AVHRR channel 2 for dust and smoke particles are due to the contamination of water vapor absorption in the computation of 6S code. Our categorization of the AERONET sites according to their prevailing aerosol types cannot be precise since the prevailing aerosol types over an AERONET site vary due to seasonal variations in the wind patterns. As a result, it would be more proper to consider the derived aerosol refractive indexes as effective ones. However, their values, compared to the error budget estimates of the aerosol optical thickness retrieval, are less dependent on satellite platforms (especially for the global ensemble case). This is because their values are determined after the systematic errors (including sensor calibration errors) included in the intercept ($A$) of the validation regression have been minimized.

[44] Our global and regional validation results indicate that the two-channel AVHRR aerosol retrieval algorithm (with globally unified aerosol model) performs well in the sense of the global mean after adjustment has been made based on the validation. It is recommended that this algorithm be implemented as NOAA/NESDIS operational aerosol retrieval algorithm. The sensitivity study indicates that the algorithm needs to be improved to make the retrieval sensitive to aerosol types and capture the aerosol regional variations observed from more advanced instruments such as the Moderate-Resolution Imaging Spectroradiometer (MODIS) on the EOS satellites. Actually, we are performing a comparison of our two-channel retrievals (using the MODIS radiance as input) with the MODIS multichannel retrievals. This will provide some insight on the compatibility between the more comprehensive MODIS aerosol retrieval and the simple long-term historical AVHRR aerosol retrieval. Results will be reported in a separate paper.

[45] Some of the procedures in the validation need to be further refined in the future. They include the following:

[46] 1. A more objective approach will be explored to find the optimal $n_r$ and $n_i$ solutions in the sensitivity studies without need a priori knowledge on the ranges of $n_r$ and $n_i$ values for the key aerosol types. The strategy should be based on selection of the average solution for the two AVHRR channels ($k$) by minimizing the quantity of $\varepsilon_{ij} = \sqrt{\frac{1}{2} \sum_{k=1}^{2} \left(1 - B_{ij}^k\right)^2}$ for the slope $B$ of the regression parameter obtained in all the combination ($ij$) of preselected $n_r$ and $n_i$.

[47] 2. Aerosol parameters for various aerosol types are also becoming available [e.g., *Dubovik et al.*, 2002a; *Smirnov et al.*, 2002b, 2003; *Procopio et al.*, 2003] through statistic analysis of multiple year AERONET observations. It is worth checking whether the global

and regional validations can be improved if these new AERONET aerosol parameters are adopted in the validation analysis.

[48] 3. AERONET observations need to be collected continuously to find sufficient matchups for validation of seasonal and monthly mean values of AVHRR aerosol retrievals at individual validation sites. As a result, the global and regional validation approaches introduced in this paper will provide useful information on the uncertainties of long-term AVHRR aerosol products in climate studies. It will also provide guidance for improving aerosol retrievals from future NOAA satellite instruments, such as the Visible/Infrared Imager Radiometer Suite (VIIRS) onboard the NPOESS satellites.

## References

Ackerman, S. A., and S. K. Cox (1989), Surface weather observations of atmospheric dust over the southeast summer monsoon region, *Meteorol. Atmos. Phys.*, *41*, 19–34.

Dave, J. V. (1973), Development of the programs for computing characteristics of ultraviolet radiation: Scalar case, *NASA Tech. Rep. NAS5-21680*, 130 pp.

Dubovik, O., and M. D. King (2000), A flexible inversion algorithm for retrieval of aerosol optical properties from Sun and sky radiance measurements, *J. Geophys. Res.*, *105*, 20,673–20,696.

Dubovik, O., B. N. Holben, T. E. Eck, A. Smirnov, Y. J. Kaufman, M. D. King, D. Tanre, and I. Slutsker (2002a), Variability of absorption and optical properties of key aerosol types observed in worldwide locations, *J. Atmos. Sci.*, *59*, 590–608.

Dubovik, O., B. N. Holben, T. Lapyonok, A. Sinyuk, M. I. Mishchenko, P. Yang, and I. Slutsker (2002b), Non-spherical aerosol retrieval method employing light scattering by spheroids, *Geophys. Res. Lett.*, *29*(10), 1415, doi:10.1029/2001GL014506.

Durkee, P. A., F. Pfeil, E. Frost, and R. Shema (1991), Global analysis of aerosol particle characteristics, *Atmos. Environ., Part A*, *25*, 2457–2471.

Galloway, J. N., and D. M. Whelpdale (1987), WATOX-86 overview and western North Atlantic Ocean S and N atmospheric budgets, *Global Biogeochem. Cycles*, *1*, 261–281.

Geogdzhayev, I. V., M. I. Mishchenko, W. B. Rossow, B. Cairns, and A. A. Lacis (2002), Global two-channel AVHRR retrievals of aerosol properties over the ocean for the period of NOAA-9 observations and preliminary retrievals using NOAA-7 and NOAA-11 data, *J. Atmos. Sci.*, *59*, 262–278.

Gross, L., R. Frouin, C. Pietras, and G. Fargion (2003), Non-supervised classification of aerosol mixtures for ocean color remote sensing, in *Proceedings of SPIE: Ocean Color Remote Sensing and Applications*, vol. 4892, edited by R. J. Frouin, Y. Yuan, and H. Kawamura, pp. 95–104, Soc. of Photo-Opt. Instr. Eng., Bellingham, Wash.

Herman, J. R., P. K. Bhartia, O. Torres, N. C. Hsu, C. J. Seftor, and E. Celarier (1997), Global distribution of UV-absorbing aerosols from Nimbus 7/TOMS data, *J. Geophys. Res.*, *102*, 16,911–16,921.

Higurashi, A., and T. Nakajima (1999), Development of a two-channel aerosol retrieval algorithm on a global scale using NOAA AVHRR, *J. Atmos. Sci.*, *56*, 924–941.

Higurashi, A., T. Nakajima, B. N. Holben, A. Smirnov, R. Frouin, and B. Chatenet (2000), A study of global aerosol optical climatology with two-channel AVHRR remote sensing, *J. Clim.*, *13*, 2011–2027.

Holben, B. N., et al. (1998), AERONET-A federated instrument network and data archive for aerosol characterization, *Remote Sens. Environ.*, *66*, 1–16.

Holben, B. N., et al. (2001), An emerging ground-based aerosol climatology: Aerosol optical depth from AERONET, *J. Geophys. Res.*, *106*, 12,067–12,097.

Hsu, N. C., J. R. Herman, O. Torres, B. N. Holben, D. Tanre, T. F. Eck, A. Smirnov, B. Chatenet, and F. Lavenu (1999), Comparisons of the TOMS aerosol index with Sun-photometer aerosol optical thickness: Results and applications, *J. Geophys. Res.*, *104*, 6269–6279.

Husar, B. R., J. M. Prospero, and L. L. Stowe (1997), Characterization of tropospheric aerosols over the oceans with the NOAA advanced very high resolution radiometer optical thickness operational product, *J. Geophys. Res.*, *102*, 16,889–16,909.

Ignatov, A., and L. L. Stowe (2000), Physical basis, premises, and self-consistency checks of aerosol retrievals from TRMM/VIRS, *J. Appl. Meteorol.*, *39*, 2259–2277.

Ignatov, A., and L. L. Stowe (2002), Aerosol retrievals from individual AVHRR channels, Part I: Retrieval algorithm and transition from Dave to 6S Radiative Transfer Model, *J. Atmos. Sci.*, *59*, 313–334.

Intergovernmental Panel on Climate Change (2001), *Climate Change 2001: The Science Basis*, 870 pp., Cambridge Univ. Press, New York.

Kaufman, Y. J., D. Tanré, O. Dubovik, A. Karnieli, and L. A. Remer (2001), Absorption of sunlight by dust as inferred from satellite and ground-based remote sensing, *Geophys. Res. Lett.*, *28*, 1479–1482.

Kaufman, Y. J., D. Tanré, and O. Boucher (2002), A satellite view of aerosols in the climate system, *Nature*, *41*, 215–223.

King, M. D., Y. J. Kaufman, D. Tanré, and T. Nakajima (1999), Remote sensing of tropospheric aerosols: Past, present, and future, *Bull. Am. Meteorol. Soc.*, *80*, 2229–2259.

Koepke, P., M. Hess, I. Schult, and E. P. Shettle (1997), Global aerosol data set, *MPI Meteorol. Hamburg Rep. 243*, 44 pp., Max-Planck-Institut, Hamburg, Germany.

Lacis, A. A., J. Chowdhary, M. I. Mishchenko, and B. Cairns (1998), Modeling errors in diffuse-sky radiation: Vector vs. scalar treatment, *Geophys. Res. Lett.*, *25*, 135–138.

Li, X., H. Maring, D. Savioe, K. Voss, and J. M. Prospero (1996), Dominance of mineral dust in aerosol light scattering in the North Atlantic trade winds, *Nature*, *380*, 416–419.

Mishchenko, M. I., I. V. Geogdzhayev, B. Cairns, W. B. Rossow, and A. Lacis (1999), Aerosol retrievals over the oceans by use of channels 1 and 2 AVHRR data: Sensitivity analysis and preliminary results, *Appl. Opt.*, *38*, 7325–7341.

Mishchenko, M. I., I. V. Geogdzhayev, L. Liu, J. A. Ogren, A. Lacis, W. B. Rossow, J. W. Hovenier, H. Volten, and O. Muòoz (2003), Aerosol retrievals from AVHRR radiances: Effects of particle nonsphericity and absorption and an updated long-term global climatology of aerosol properties, *J. Quant. Spectrosc. Radiat. Transfer.*, *79–80*, 953–972.

Patterson, E. M., D. A. Gillette, and B. H. Stockton (1977), Complex index of refraction between 300 and 700 for Saharan aerosols, *J. Geophys. Res.*, *82*, 3153–3160.

Procopio, A. S., L. A. Remer, P. Artaxo, Y. J. Kaufman, and B. N. Holben (2003), Modeled spectral optical properties for smoke aerosols in Amazonia, *Geophys. Res. Lett.*, *30*(24), 2265, doi:10.1029/2003GL018063.

Prospero, J. M., R. Schmitt, E. Cuevas, D. L. Savoie, W. C. Graustein, K. K. Turekian, A. Volz-Thmas, A. D. Diaz, S. J. Oltmans, and H. Levy II (1995), Temporal variability of summertime ozone and aerosols in the free troposphere over the eastern North Atlantic, *Geophys. Res. Lett.*, *22*, 2925–2928.

Prospero, J. M., D. L. Savoie, R. Arimoto, H. Olafsson, and H. Hjartarson (1995b), Sources of aerosol nitrate and non-sea-salt (nss) sulfate in the Iceland region, *Sci. Total Environ.*, *160/161*, 181–191.

Redemann, J., et al. (2000), Retrieving the vertical structure of the effective aerosol complex index of refraction from a combination of aerosol in situ and remote sensing measurements during TARFOX, *J. Geophys. Res.*, *105*, 9949–9970.

Remer, L. A., Y. J. Kaufman, and B. N. Holben (1999), Interannual variation of ambient aerosol characteristics on the east coast of the United States, *J. Geophys. Res.*, *104*, 2223–2231.

Shettle, E. P., and R. W. Fenn (1979), Models of aerosols of lower troposphere and the effect of humidity variations on their optical properties, *AFCRL Tech. Rep. 790214*, 100 pp., Air Force Cambridge Res. Lab., Hanscom Air Force Base, Mass.

Smirnov, A., B. N. Holben, T. F. Eck, O. Dubovik, and I. Slutsker (2000), Cloud screening and quality control algorithms for the AERONET data base, *Remote Sens. Environ.*, *73*, 337–349.

Smirnov, A., B. N. Holben, O. Dubovik, N. T. O'Neill, T. F. Eck, D. L. Westphal, A. K. Goroch, C. Pietras, and I. Slutsker (2002a), Atmospherical aerosol optical properties in the Persian Gulf region, *J. Atmos. Sci.*, *59*, 620–634.

Smirnov, A., B. N. Holben, Y. J. Kaufman, O. Dubovik, T. F. Eck, I. Slutsker, C. Pietras, and R. Halthore (2002b), Optical properties of atmospheric aerosol in maritime environments, *J. Atmos. Sci.*, *59*, 501–523.

Smirnov, A., B. N. Holben, O. Dubovik, R. Frouin, T. F. Eck, and I. Slutsker (2003), Maritime component in aerosol optical models derived from

Aerosol Robotic Network data, *J. Geophys. Res.*, *108*(D1), 4033, doi:10,1029/2002JD002701.

Sokolik, I., and O. B. Toon (1999), Incorporation of mineralogical composition into models of the radiative properties of mineral aerosol from UV to IR wavelengths, *J. Geophys. Res.*, *104*, 9423–9444.

Sokolik, I., A. Andronove, and T. C. Johnson (1993), Complex refractive index of atmospheric dust aerosols, *Atmos. Environ., Part A*, *27*, 2495–2502.

Stowe, L. L., A. M. Ignatov, and R. R. Sigh (1997), Development, validation, and potential enhancements to the second-generation operational aerosol product at the National Environmental Satellite, Data, and Information Service of the National Oceanic and Atmospheric Administration, *J. Geophys. Res.*, *102*, 16,923–16,932.

Tanré, D., B. N. Holben, and Y. J. Kaufman (1992), Atmospheric correction algorithm for NOAA-AVHRR products: Theory and applications, *IEEE Trans. Geosci. Remote Sens.*, *30*, 231–248.

Tanré, D., M. Herman, and Y. J. Kaufman (1996), Information on the aerosol size distribution contained in the solar reflected spectral radiances, *J. Geophys. Res.*, *101*, 19,043–19,060.

Tanré, D., Y. J. Kaufman, B. N. Holben, B. Chatenet, A. Karnieli, F. Lavenu, L. Blarel, O. Dubovik, L. A. Remer, and A. Smirnov (2001), Climatology of dust aerosol size distribution and optical properties derived from remotely sensed data in the solar spectrum, *J. Geophys. Res.*, *106*, 18,205–18,218.

Torres, O., P. K. Bhartia, J. R. Herman, Z. Ahmad, and J. Gleason (1998), Derivation of aerosol properties from satellite measurements of backscattered ultraviolet radiation: Theoretical basis, *J. Geophys. Res.*, *103*, 17,099–17,110.

Torres, O., P. K. Bhartia, J. R. Herman, A. Sinyuk, P. Ginoux, and B. Holben (2002), A long-term record of aerosol optical depth from TOMS observations and comparison to AERONET measurements, *J. Atmos. Sci.*, *59*, 398–413.

Vermote, E., D. Tanre, J. L. Deuze, M. Herman, and J. J. Morcrette (1997), Second simulation of the satellite signal in the solar spectrum, "6S": An overview, *IEEE Trans. Geosci. Remote Sens.*, *35*, 675–686.

World Meteorological Organization (1983), Radiation commission of IAMAP meeting of experts on aerosol and their climatic effects, *Rep. WCP55*, pp. 28–30, Williamsburg Va.

Zhao, X., L. L. Stowe, A. Smirnov, D. Crosby, J. Sapper, and C. R. McClain (2002), Development of a global validation package for satellite oceanic aerosol optical thickness retrieval based on AERONET observations and its application to NOAA/NESDIS operational aerosol retrievals, *J. Atmos. Sci.*, *59*, 294–312.

Zhao, X., I. Laszlo, B. N. Holben, C. Pietras, and K. J. Voss (2003a), Validation of two-channel VIRS retrievals of aerosol optical thickness over ocean and quantitative evaluation of the impact from potential sub-pixel cloud contamination and surface wind effect, *J. Geophys. Res.*, *108*(D3), 4106, doi:10.1029/2002JD002346.

Zhao, T. X.-P., I. Laszlo, O. Dubovik, B. N. Holben, J. Sapper, D. Tanré, and C. Pietras (2003b), A study of the effect of non-spherical dust particles on the AVHRR aerosol optical thickness retrievals, *Geophys. Res. Lett.*, *30*(6), 1317, doi:10.1029/2002GL016379.

————————————

O. Dubovik and A. Smirnov, Goddard Earth Sciences and Technology Center, University of Maryland Baltimore Campus, Goddard Space Flight Center, Greenbelt, MD 20771, USA.

R. Frouin, Scripps Institution of Oceanography, University of California San Diego, 8605 La Jolla Shore Drive, La Jolla, CA 92037, USA.

B. N. Holben, Laboratory for Terrestrial Physics, NASA/GSFC, Code 923, Greenbelt, MD 20771, USA.

C. Pietras, SAIC, NASA/GSFC, Code 970.2, Greenbelt, MD 20771, USA.

J. Sapper, NOAA/NESDIS/OSDPD, Suitland, MD 20746, USA.

K. J. Voss, Department of Physics, University of Miami, Coral Gables, FL 33124, USA.

T. X.-P. Zhao, E/RA1, RM 7121, WWBG, NOAA/NESDIS/ORA, 5200 Auth Road, Camp Springs, MD 20746, USA. (xuepeng.zhao@noaa.gov)